



## Article

# Higher Activity of Ni/ $\gamma$ -Al<sub>2</sub>O<sub>3</sub> over Fe/ $\gamma$ -Al<sub>2</sub>O<sub>3</sub> and Ru/ $\gamma$ -Al<sub>2</sub>O<sub>3</sub> for Catalytic Ammonia Synthesis in Nonthermal Atmospheric-Pressure Plasma of N<sub>2</sub> and H<sub>2</sub>

Masakazu Iwamoto <sup>1,\*</sup> , Masataka Horikoshi <sup>2</sup>, Ryu Hashimoto <sup>2</sup>, Kaori Shimano <sup>2</sup>, Tomiko Sawaguchi <sup>1</sup>, Harunobu Teduka <sup>1</sup> and Masahiko Matsukata <sup>1</sup> 

<sup>1</sup> Research Institute for Science and Engineering, Waseda University, 3-4-1 Okubo, Sinjuku-ku, Tokyo 169-8555, Japan; t.sawaguchi3@kurenai.waseda.jp (T.S.); hazel.wand.0321@gmail.com (H.T.); mmatsu@waseda.jp (M.M.)

<sup>2</sup> Department of Applied Chemistry, Faculty of Science and Engineering, Chuo University, 1-13-27 Kasuga, Bunkyo-ku, Tokyo 112-8551, Japan; resque6411@gmail.com (M.H.); hryu.03002h@gmail.com (R.H.); kaori.shimano.23@gmail.com (K.S.)

\* Correspondence: rockbasejp@gmail.com; Tel.: +81-3-5286-3115

Received: 6 May 2020; Accepted: 22 May 2020; Published: 25 May 2020



**Abstract:** Developing a novel ammonia synthesis process from N<sub>2</sub> and H<sub>2</sub> is of interest to the catalysis and hydrogen research communities.  $\gamma$ -Alumina-supported nickel was determined capable of serving as an efficient catalyst for ammonia synthesis using nonthermal plasma under atmospheric pressure without heating. The catalytic activity was almost unrelated to the crystal structure and the surface area of the alumina carrier. The activity of Ni/Al<sub>2</sub>O<sub>3</sub> was quantitatively compared with that of Fe/Al<sub>2</sub>O<sub>3</sub> and Ru/Al<sub>2</sub>O<sub>3</sub>, which contained active metals for the conventional Haber–Bosch process. The activity sequence was Ni/Al<sub>2</sub>O<sub>3</sub> > Al<sub>2</sub>O<sub>3</sub> > Fe/Al<sub>2</sub>O<sub>3</sub> > no additive > Ru/Al<sub>2</sub>O<sub>3</sub>, surprisingly indicating that the loading of Fe and Ru decreased the activity of Al<sub>2</sub>O<sub>3</sub>. The catalytic activity of Ni/Al<sub>2</sub>O<sub>3</sub> was dependent on the amount of loaded Ni, the calcination temperature, and the reaction time. XRD, visual, and XPS observations of the catalysts before the plasma reaction indicated the generation of NiO and NiAl<sub>2</sub>O<sub>4</sub> on Al<sub>2</sub>O<sub>3</sub>, the latter of which was generated upon high-temperature calcination. The NiO species was readily reduced to Ni metal in the plasma reaction, whereas the NiAl<sub>2</sub>O<sub>4</sub> species was difficult to reduce. The catalytic behavior could be attributed to the production of fine Ni metal particles that served as active sites. The P<sub>N2</sub>/P<sub>H2</sub> ratio dependence and rate constants of formation and decomposition of ammonia were finally determined for 5.0 wt% Ni/Al<sub>2</sub>O<sub>3</sub> calcined at 773 K. The ammonia yield was 6.3% at an applied voltage of 6.0 kV, a residence time of reactant gases of 0.12 min, and P<sub>H2</sub>/P<sub>N2</sub> = 1.

**Keywords:** ammonia synthesis; nonthermal plasma; atmospheric pressure; nickel; alumina

## 1. Introduction

New methods for the synthesis of ammonia have been widely investigated in many catalysis fields to improve or displace the current Haber–Bosch process due to its extreme reaction conditions and high consumption of energy supply. In the field of heterogeneous catalysis, new catalytic systems, including mainly Ru as an active site, were reported [1–11]. However, relatively high yields were usually accompanied by low reaction rates, while high reaction rates were accompanied by low yields. At present, such a trade-off correlation is very difficult to overcome. In the field of homogeneous catalysis [12–16], various metal complexes were reported to be active for ammonia

synthesis. The turnover numbers of the recently reported catalysts were 100–200, indicating the need for extensive research efforts to make a practical system. Electrocatalysis was also reported using Ag-Pd alloys and Ru/supports as electrode catalysts [17–23], but their reaction rates were far lower than those of the Haber–Bosch process. In catalysis using nonthermal atmospheric-pressure plasma for the activation of a nitrogen molecule [24–34], Ru- or Fe-loaded ceramic membranes or metal oxides such as BaTiO<sub>3</sub> were used, and the yields reached a few percent. However, the production rates were slow, due to the slow-flowing velocity of the reactant gases via the ceramic layers [34–37].

In contrast, we have recently reported that a wool-like metal electrode, used to produce nonthermal plasma, functioned as an efficient catalyst for ammonia production from N<sub>2</sub> and H<sub>2</sub> under atmospheric pressure without heating [38,39]. The order of activity at each initial experiment was Au > Pt > Pd > Ag > Cu > Fe > Mo > Ni > W > Ti > Al [39]. Most of the metals were not reported as active for ammonia synthesis in the Haber–Bosch process. After the activity was stabilized by repeated experiments, the ammonia yield was 3.5% at H<sub>2</sub>/N<sub>2</sub> = 3 on copper [38], which was the highest among the values reported at atmospheric pressure. In a typical Haber–Bosch process, the triple bond between the two nitrogen atoms is activated by electron donation from the catalyst. However, in the plasma process, the nitrogen molecule is activated by the plasma, and the catalyst provides the reaction site for the activated species. Although a detailed ammonia synthesis mechanism for the plasma catalysis remained unclear, these new findings made us consider that some metal oxides might also be active for this reaction.

Various nickel-containing materials have been reported to be active for the catalytic decomposition of ammonia [40–46]. Since the ammonia decomposition reaction is an equilibrium reaction at a middle temperature range, these earlier works might suggest the possibility of the nickel-containing materials working as active catalysts for ammonia synthesis. In fact, several nickel-containing nitride compounds have been reported as active for ammonia synthesis [47–51], although very severe reaction conditions, such as high reaction temperature and high pressure, were often required. In the current work, the catalytic activity of nickel-supported alumina was studied in a nonthermal atmospheric pressure plasma without any heating and compared with those of iron- or ruthenium-supported alumina that are well-known to be active for the conventional Haber–Bosch process. We found that the activity of Ni/Al<sub>2</sub>O<sub>3</sub> was much higher than that of Fe/Al<sub>2</sub>O<sub>3</sub> and Ru/Al<sub>2</sub>O<sub>3</sub>, and surprisingly, the activities of the latter two compounds were lower than that of alumina alone. The dependencies of the ammonia synthesis on the P<sub>H2</sub>/P<sub>N2</sub> ratio and the residence time of the reactant gases were also studied on Al<sub>2</sub>O<sub>3</sub> and 5.0 wt% Ni/Al<sub>2</sub>O<sub>3</sub> calcined at 773 K. The new reaction system effectively produced ammonia with yields of 3.0% and 6.3% on the catalysts at a residence time of reactant gases of 0.12 min and P<sub>H2</sub>/P<sub>N2</sub> = 1. This method provides new insights into ammonia synthesis that will be significant for the future hydrogen economy.

## 2. Results and Discussion

### 2.1. Comparison of the Activities of Various Oxide Catalysts

It has been reported that alumina, used as a carrier in this study, shows catalytic activity for the plasma synthesis of ammonia. In this study, we first compared the catalytic activity of alumina as a function of surface area and crystal structure. The results are summarized in Figure 1, in which the supplier of alumina, sample name, surface area, and amount used in plasma experiments are listed in Table S1 (in Supporting Information). In the reaction conditions, H<sub>2</sub>/N<sub>2</sub> means the ratio of partial pressure of supplied H<sub>2</sub> and that of supplied N<sub>2</sub>. The horizontal axis of the figure is the total surface area of alumina actually used in the catalyst experiment. The colors of the plots indicate that the structure of alumina is alpha-type (yellow), theta (white), gamma (red), or a mixture of theta and gamma (blue). The red broken line indicates the average activity of all Al<sub>2</sub>O<sub>3</sub>. It is clear that the catalytic activity did not change significantly depending on the crystal structure or surface area,

although it did change somewhat. In this study, we employed gamma-type alumina as the support because it has a medium-high surface area and the crystal structure is stable.

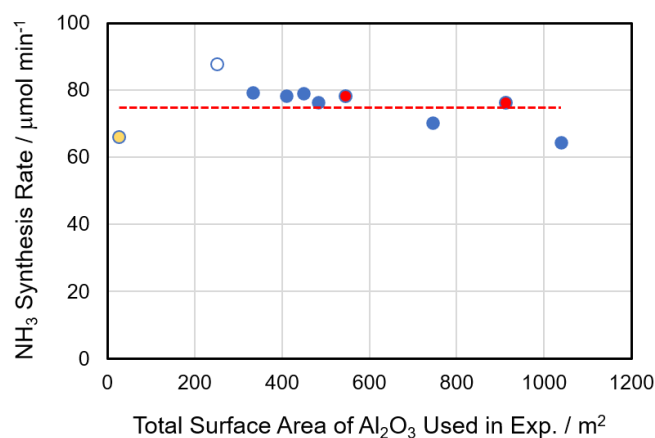


**Figure 1.** Comparison of activities of various Al<sub>2</sub>O<sub>3</sub> as a function of total surface area and crystal structure. The crystal structure of  $\alpha$ ,  $\theta$ ,  $\gamma$ , and  $\theta + \gamma$  is shown by yellow, white, red, and blue plots. The red broken line is the average NH<sub>3</sub> synthesis rate. Reaction conditions: applied voltage, 6 kV; frequency, 50 kHz; electrode length, 150 mm; total flow rate, 100 mL min<sup>-1</sup>; and H<sub>2</sub>/N<sub>2</sub> = 1.

The catalytic activities of Ni/Al<sub>2</sub>O<sub>3</sub> were quantitatively compared with the activities of Fe/Al<sub>2</sub>O<sub>3</sub> and Ru/Al<sub>2</sub>O<sub>3</sub> in Figure 2, where the components listed in the figure were determined by XRD measurements after the reactions. The amounts of loaded metals were all 5.0 wt% as metal, which are indicated by the first numerical values of the sample names. KC and SC mean  $\gamma$ -Al<sub>2</sub>O<sub>3</sub> purchased from Kanto Chemical Co., Japan, and Strem Chemicals Inc., USA, and the numerical values such as 773 are the calcination temperatures of catalysts in Kelvin. At first, it should be noted that the activities of Al<sub>2</sub>O<sub>3</sub>(SC) and Al<sub>2</sub>O<sub>3</sub>(KC) were similar and that the activities of 5Ni/Al<sub>2</sub>O<sub>3</sub>(SC, 773) and 5Ni/Al<sub>2</sub>O<sub>3</sub>(KC, 773) were also similar, although the former comparison was already shown in Figure 1. The results ensured again that there was no problem in using either the SC or KC alumina as the carrier without distinction. The activities of the catalysts were in the following order 5Ni/Al<sub>2</sub>O<sub>3</sub> > Al<sub>2</sub>O<sub>3</sub> > 5Fe/Al<sub>2</sub>O<sub>3</sub> > no additive (a blank experiment) > 5Ru/Al<sub>2</sub>O<sub>3</sub>, surprisingly indicating that the loading of iron and ruthenium decreased the activity of Al<sub>2</sub>O<sub>3</sub>. As indicated in the introduction, the plasma atmosphere works as a preactivation port of nitrogen and hydrogen molecules, and the catalysts should work as a reaction port of preactivated molecules. Fe and Ru would not be useful for this purpose, although they are active for activation of the triple bond between two nitrogen atoms. It is widely accepted in the Haber–Bosch process that Fe and Ru can gather hydrogen atoms adsorbed on supports and exhibit high activity for their reaction with a nitrogen atom activated on the metal site. The loading of Fe or Ru might decrease the number of hydrogen atoms on alumina, which resulted in smaller ammonia yields than that of alumina alone. The results also suggested that there will be many opportunities in the field to develop an active catalyst for ammonia synthesis from preactivated nitrogen with hydrogen, as well as revealing the reaction mechanism and active species.

Recently a spillover rate of a hydrogen atom on titania was reported to be much faster than that on alumina by DFT calculations [52] and experimental measurements [53]. The surface diffusion of a hydrogen atom might be important for the catalytic ammonia synthesis using the plasma atmosphere. TiO<sub>2</sub> particles (diameter of 0.3–0.6  $\mu$ m, a rutile type) purchased from Kanto Chemical Co., Japan was used as a parent catalyst and 5.0 wt% of Ni was loaded on TiO<sub>2</sub> in a similar manner to that in the preparation of 5Ni/Al<sub>2</sub>O<sub>3</sub>. TiO<sub>2</sub> and 5Ni/TiO<sub>2</sub> were employed as catalysts for the plasma ammonia synthesis after calcination at 773 K for 4 h in air. The formation rates of ammonia on TiO<sub>2</sub> and 5Ni/TiO<sub>2</sub> were 32.7 and 45.0  $\mu$ mol min<sup>-1</sup>, respectively, at H<sub>2</sub>/N<sub>2</sub> = 1, total flow rate = 100 mL min<sup>-1</sup>, 6 kV, and 50 kHz (a typical reaction condition same as those applied for 5Ni/Al<sub>2</sub>O<sub>3</sub>). No deactivation was

observed on the catalysts. Unfortunately, the ammonia formation rates were lower than those of  $\text{Al}_2\text{O}_3$  and  $5\text{Ni}/\text{Al}_2\text{O}_3$  catalysts. The catalytic activity was compared with various parameters of oxides such as a relative dielectric constant [34] and a lattice constant, but no clear correlation could be found for explanation of the catalysis.

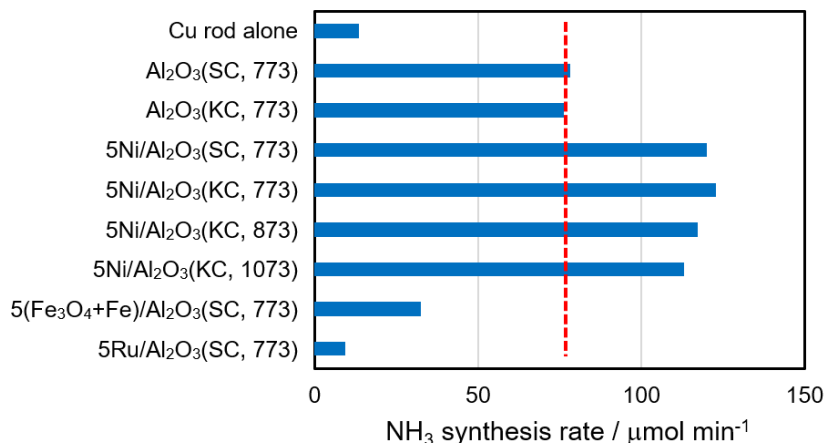


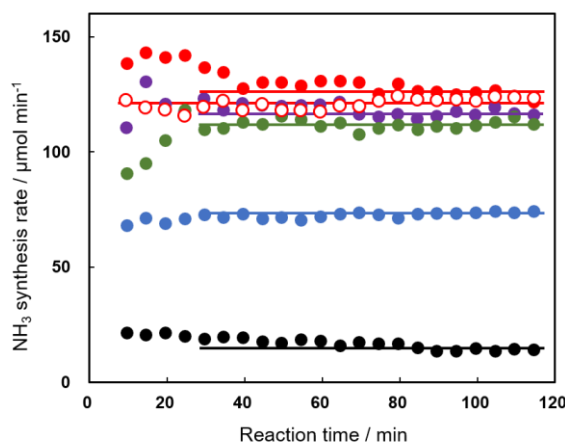
**Figure 2.** Comparison of activities of Ni-, Fe-, and Ru-supported  $\gamma\text{-Al}_2\text{O}_3$  catalysts. The red broken line indicates the average activity of  $\text{Al}_2\text{O}_3(\text{SC})$  and  $\text{Al}_2\text{O}_3(\text{KC})$ . Reaction conditions were the same as those in Figure 1.

## 2.2. Activity and Active Sites of $\text{Ni}/\text{Al}_2\text{O}_3$ for Ammonia Synthesis

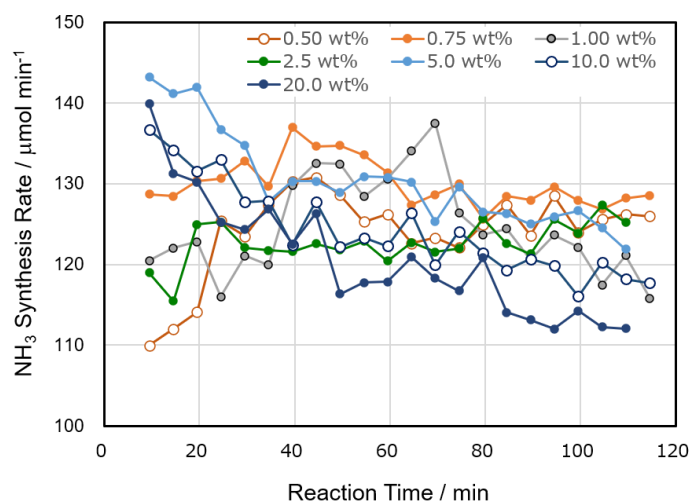
The catalytic activities of  $\text{Al}_2\text{O}_3(\text{KC})$  and  $\text{Ni}/\text{Al}_2\text{O}_3(\text{KC})$  were studied as a function of reaction time and amount of loaded nickel, and typical ammonia synthesis rates are summarized in Figures 3 and 4 together with the activity of a Cu inner electrode alone (the experiment is called “a blank test” hereafter). As shown in Figure 3, the catalytic activity of the blank test slightly decreased with reaction time, although the reason for the change remained unknown. Additionally, the activity of the ammonia synthesis increased by using  $\text{Al}_2\text{O}_3$  as the catalyst and further improved when Ni was supported on  $\text{Al}_2\text{O}_3$ . The activity of the  $\text{Ni}/\text{Al}_2\text{O}_3$  catalyst changed with the amount of Ni loaded, the calcination temperature, and the reaction time. The activities of  $\text{Ni}/\text{Al}_2\text{O}_3(\text{KC}, 773)$  catalysts containing 0.50–20.0 wt% Ni showed characteristic changes with reaction time (Figure 4). When the amount of Ni loaded was small (0.50–1.00 wt%), the activity increased in the early stage of the reaction, reached the maximum activity, and then decreased. In contrast, the activities of 5.0–20.0 wt%  $\text{Ni}/\text{Al}_2\text{O}_3(\text{KC}, 773)$  were high in the initial stages and gradually decreased with the reaction time. Only 2.5 wt%  $\text{Ni}/\text{Al}_2\text{O}_3(\text{KC}, 773)$  showed almost constant activity. As will be shown in the following section, we proposed that these activity enhancements and reductions were caused by changes in the Ni state on the support by the plasma irradiation. The second important observation in Figure 4 is that the catalytic activity is almost independent of the amount of loaded Ni. We will suggest that a very small amount of Ni functions as a catalytically active site, and that the amount does not change with increasing Ni loading.

Figure 3 summarizes the effect of calcination temperature, where a 5.0 wt% sample was employed for this study, since the characterization of Ni would become difficult when the amount of Ni supported was too small. Although the activity of  $5\text{Ni}/\text{Al}_2\text{O}_3(\text{KC}, 773)$  decreased with the reaction time, as also shown in Figure 4, it was confirmed, in the second experiment (open red circles in Figure 3) on the catalyst once used, that the activity stabilized at approximately  $120 \mu\text{mol min}^{-1}$  after a 2 h reaction. On  $5\text{Ni}/\text{Al}_2\text{O}_3(\text{KC}, 873)$ , the activity gradually decreased, although the degree of decrease was smaller than that on  $5\text{Ni}/\text{Al}_2\text{O}_3(\text{KC}, 773)$ . On the other hand, the behavior of  $5\text{Ni}/\text{Al}_2\text{O}_3(\text{KC}, 1073)$  was essentially different from those of the above two catalysts. The activity increased at the initial stage, then stabilized after a reaction time of 30 min. It should be noted that the activities on the three

catalysts nearly agreed at approximately  $120 \mu\text{mol min}^{-1}$  at 120 min, which was similar to those observed in Figure 4.



**Figure 3.** Time courses for the catalytic activities of the copper rod (black),  $\text{Al}_2\text{O}_3(\text{KC})$  (blue), and  $5\text{Ni}/\text{Al}_2\text{O}_3(\text{KC}, 773)$  (closed red, the 1st run; open red, the 2nd run on the same catalyst),  $5\text{Ni}/\text{Al}_2\text{O}_3(\text{KC}, 873)$  (purple), and  $5\text{Ni}/\text{Al}_2\text{O}_3(\text{KC}, 1073)$  (green) for the plasma synthesis of ammonia. Reaction conditions were the same as those in Figure 1.



**Figure 4.** Time courses for the catalytic activities of  $\text{Al}_2\text{O}_3$ -loaded Ni catalysts (KC, 773) for the plasma synthesis of ammonia. The amounts of loaded Ni are shown in the figure. Reaction conditions were the same as those in Figure 1.

These changes were attributed to changes in the nickel species, resulting from the calcination temperature and the reductive atmosphere of the plasma experiment. The X-ray diffraction patterns of  $\text{Ni}/\text{Al}_2\text{O}_3$  [51–56] were measured before and after the reaction shown in Figure 3, and the results are summarized in Figure 5. XRD peaks of the  $\gamma$ -alumina carrier appeared at  $2\theta = 38, 45,$  and  $67$  degrees, assignable to the diffractions from (311), (400), and (440) faces, and the pattern was almost the same as that of  $5\text{Ni}/\text{Al}_2\text{O}_3(\text{KC}, 773)$  before the plasma reaction (Figure 5a), although not shown in the figure for simplicity. Before the catalysts were used in the plasma reaction, diffraction peaks attributable to the  $\text{NiO}$  phase ( $2\theta = 43$  and  $63$  degrees) could hardly be observed as clear peaks on the three samples. The peaks of  $\text{NiAl}_2\text{O}_4$  ( $2\theta = 19.1, 31.4, 37.0, 45.0, 55.3, 59.7,$  and  $65.5$  degrees) were observed on the 873 K and 1073 K calcined samples. The findings were in good agreement with reports that the  $\text{NiAl}_2\text{O}_4$  formation from  $\text{NiO}$  and  $\text{Al}_2\text{O}_3$  begins upon calcination at 723 K [57] and becomes vigorous at 873 K and above. The respective colors of  $5\text{Ni}/\text{Al}_2\text{O}_3$  calcined at 773, 873, and 1073 K were pale

greenish-gray, light sky blue, and pale blue; these corresponded well to the pale green-pale gray of NiO (depending on the oxygen content) and the pale blue of  $5\text{NiAl}_2\text{O}_4$  [58], again indicating the production of these oxides on alumina. Upon the plasma experiments, the XRD patterns and the sample colors were changed. On the used  $5\text{Ni}/\text{Al}_2\text{O}_3(\text{KC}, 773)$ , the formation of Ni metal particles was confirmed with the XRD peaks of  $2\theta = 44.5, 52,$  and  $76$  degrees [49,50], although their intensities were very small. The diffraction peaks originating from NiO disappeared at the same time. On the used  $5\text{Ni}/\text{Al}_2\text{O}_3(\text{KC}, 873)$  and  $5\text{Ni}/\text{Al}_2\text{O}_3(\text{KC}, 1073)$ , the XRD peaks of metallic Ni did not appear irrespective of the disappearance of the NiO peaks, which could be due to the formation of small Ni particles. The sample colors were greatly changed. Black, gray, and grayish pale blue were the colors for the used  $5\text{Ni}/\text{Al}_2\text{O}_3(\text{KC}, 773)$ ,  $5\text{Ni}/\text{Al}_2\text{O}_3(\text{KC}, 873)$ , and  $5\text{Ni}/\text{Al}_2\text{O}_3(\text{KC}, 1073)$ , respectively. The color changes supported the formation of metallic Ni (black), which was shown in the XRD experiments.

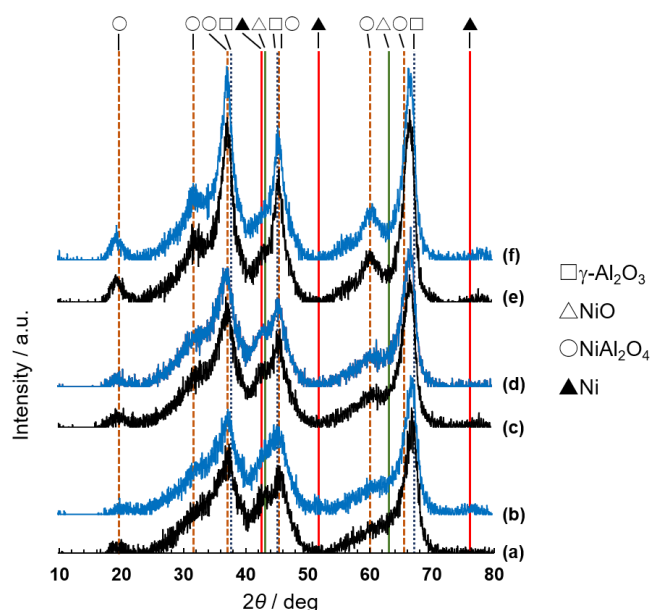


**Figure 5.** XRD patterns of  $5\text{Ni}/\text{Al}_2\text{O}_3(\text{KC}, 773)$  (a,b),  $5\text{Ni}/\text{Al}_2\text{O}_3(\text{KC}, 873)$  (c,d), and  $5\text{Ni}/\text{Al}_2\text{O}_3(\text{KC}, 1073)$  (e,f) before (black) and after (blue) the plasma experiments shown in Figure 3. The diffraction lines could be assigned to  $\gamma\text{-Al}_2\text{O}_3$  (open square), NiO (open triangle),  $\text{NiAl}_2\text{O}_4$  (open circle), and metallic Ni particles (closed triangle).

For the ammonia synthesis in the plasma atmosphere, the following active sites were suggested based on the above observations. The reduction of NiO to Ni occurred very easily with activated hydrogen molecules to form atomically dispersed Ni metal particles, the resultant very small Ni particles were converted to fine particles of Ni metal, and finally, the fine particles gathered slowly to form large particles. The fine particles were active for the ammonia synthesis, while large Ni particles were not. The low catalytic activity of large Ni particles was supported by the previous finding that wool-like Ni metal wires showed very low catalytic activity for the reaction [39]. With  $5\text{Ni}/\text{Al}_2\text{O}_3(\text{KC}, 773)$ , the formation of fine Ni fine particles [55] finished immediately after the plasma reaction started because of the facile reducibility of NiO. The prolonged reaction time, however, caused agglomeration of the Ni particles, which induced a decrease in the catalytic activity, as shown in Figures 3 and 4. With  $5\text{Ni}/\text{Al}_2\text{O}_3(\text{KC}, 1073)$ , the NiO on the surface was reduced to Ni particles, but the number of the atomically dispersed particles was smaller than that on  $5\text{Ni}/\text{Al}_2\text{O}_3(\text{KC}, 773)$  due to the limited amount of supported Ni, which was loaded as both NiO and  $\text{NiAl}_2\text{O}_4$ . Since the reduction of  $\text{NiAl}_2\text{O}_4$  was difficult under the present reaction conditions [55,59], the number of fine Ni particles gradually increased during the reaction by moving of the atomically dispersed particles, which resulted in the increase in the catalytic activity for the first 30 min, as shown in Figure 3. After the 120 min reaction,



the changes in catalytic activity on the three catalysts nearly disappeared, and they reached nearly the same conversion level. The similar changes in activities can be observed on the Ni/Al<sub>2</sub>O<sub>3</sub>(KC, 773) catalysts with low amounts of loaded Ni. As shown in Figure 4, the activities of catalysts with Ni contents of 0.50–1.00 wt% increased in the early stage of the reaction, reached the respective maximum values, and then decreased. The phenomena could be explained with the changes of Ni particles from very small ones to fine ones and then to large ones. In the present discussion, the active phase was assumed to be fine particles, but it might be particles with an amorphous structure.

The above discussion was supported by the XPS characterization of the catalysts. The XPS spectra of 5Ni/Al<sub>2</sub>O<sub>3</sub>(KC, 1073) are summarized in Figure 6 as typical examples. The Ni 2p<sub>3/2</sub> peaks were reported to appear at 852, 854–855, and 856–857 eV together with satellite peaks [60–64], which could be attributed to Ni<sup>0</sup> (metal), Ni<sup>2+</sup> of NiO, and Ni<sup>2+</sup> of NiAl<sub>2</sub>O<sub>4</sub> (a spinel compound), respectively. With the present 5Ni/Al<sub>2</sub>O<sub>3</sub>(KC, 1073), three peaks were observed at 852.5, 855.0, and 856.1 eV before and after the reaction, as shown in Figure 6, indicating the formation of Ni metal, NiO, and NiAl<sub>2</sub>O<sub>4</sub> species. The intensity ratios of the three peaks were approximately 0:37:63 before the reaction and 38:0:62 after the reaction. The findings indicated the easy and quantitative reduction of NiO to Ni<sup>0</sup> and the difficult reduction of NiAl<sub>2</sub>O<sub>4</sub>, which were in good agreement with behaviors observed in reforming reactions [55,56]. With 5Ni/Al<sub>2</sub>O<sub>3</sub>(KC, 773), only NiO was observed before the plasma reaction, with nearly all of the species being reduced to Ni metal after the reaction. The XPS spectra of 5Ni/Al<sub>2</sub>O<sub>3</sub>(KC, 873) revealed a change in the ratio of Ni metal, NiO, and NiAl<sub>2</sub>O<sub>4</sub> from 0:81:19 to 83:0:17 before and after the reaction. All findings supported the discussion in the previous section that Ni metal on the alumina support, produced by the reduction of NiO in the plasma reaction, would be active for the ammonia synthesis, although the XRD peaks attributable to Ni metal were not clearly recognized.

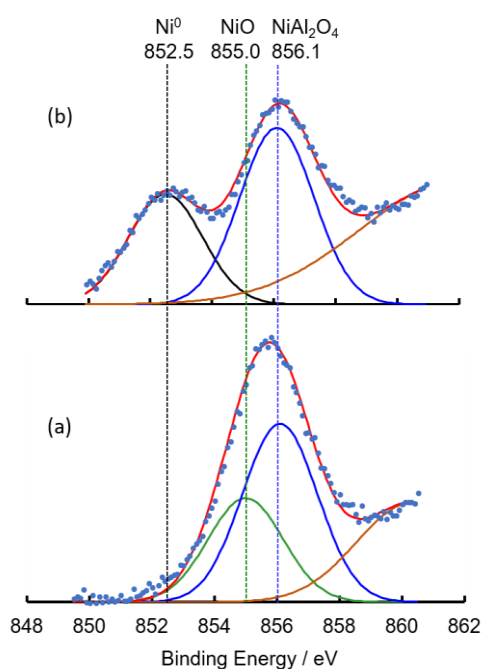


**Figure 6.** XPS spectra of Ni 2p<sub>3/2</sub> for 5Ni/Al<sub>2</sub>O<sub>3</sub>(KC, 1073) before (a) and after (b) the plasma experiments shown in Figure 3. The blue points are the measured values. The deconvolution showed the presence of NiO (green), NiAl<sub>2</sub>O<sub>4</sub> (blue), and metallic Ni species (black) with a base line (brown) including satellite peaks. The red lines are the sums of the respective calculated lines.

### 2.3. Kinetic Analysis of Ammonia Synthesis on Ni/Al<sub>2</sub>O<sub>3</sub>

The ammonia synthesis rates and yields on Al<sub>2</sub>O<sub>3</sub> and 5Ni/Al<sub>2</sub>O<sub>3</sub>(KC, 773) were examined as a function of the molar ratio of H<sub>2</sub> and N<sub>2</sub> (Figure 7). The synthesis rates were maximized

at  $H_2/N_2 = 2$  and 1 on  $Al_2O_3$  and  $5Ni/Al_2O_3$ , respectively, and reached 93 and 121  $\mu\text{mol min}^{-1}$ . The respective yields increased monotonously as the  $H_2/N_2$  ratio increased due to a decrease in the concentration of the introduced  $N_2$ . The yields reached 4.1% and 4.6% at  $H_2/N_2 = 3$  (the stoichiometric ratio for ammonia synthesis) on  $Al_2O_3$  and  $5Ni/Al_2O_3$ , respectively. The synthesis rates and yields were greater than those observed in previous metal wire systems [38,39]. To investigate the dependencies on the individual concentrations in a gas-phase reaction, we usually used inert gases such as helium or argon to adjust the respective partial pressures. However, it has been widely reported for plasma reactions that these gases show the remarkable Penning effect, which largely changes the experimental results. Thus, we had to perform the experiments using a mixture of only  $N_2$  and  $H_2$  without any diluent. The correlation in Figure 7 was analyzed using the following kinetic equation, where the reaction rate was expressed using a power equation.

$$r_{NH_3} = kP_{H_2}^{\alpha}P_{N_2}^{\beta} \quad (1)$$

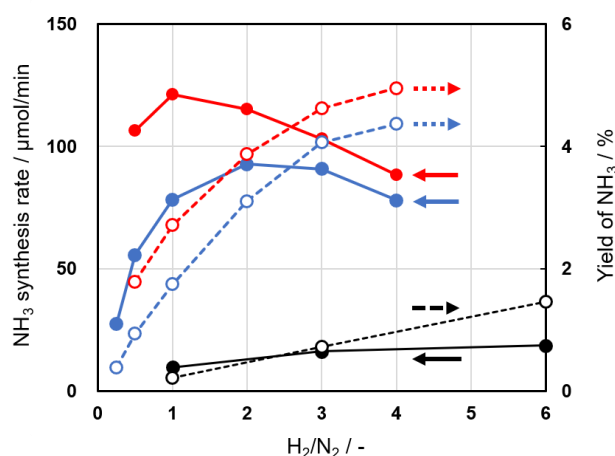


**Figure 7.** Change in the synthesis rate (closed) and yield (open) of ammonia as a function of the  $N_2/H_2$  ratio using  $Al_2O_3(SC)$  (blue) and  $5Ni/Al_2O_3(KC, 773)$  (red) catalysts. The results of the blank experiment (black) are also shown for comparison. Reaction conditions: applied voltage, 6 kV; frequency, 50 kHz; electrode length, 150 mm; total flow rate, and 100  $\text{mL min}^{-1}$ .

A least-squares method was applied to determine the  $\alpha$  and  $\beta$  values.  $\alpha(Al_2O_3(SC)) = 1.59$ ,  $\beta(Al_2O_3(SC)) = 0.82$  and  $\alpha(5Ni/Al_2O_3(KC, 773)) = 1.12$ ,  $\beta(5Ni/Al_2O_3(KC, 773)) = 0.99$  were obtained from the calculations. These values differed from those reported on well-known solid catalysts ( $\alpha = 1.5\text{--}2.2$  and  $\beta = 0.9\text{--}1.2$  on Fe, and  $\alpha = -0.43$  and  $\beta = 1.0$  on Ru-Cs/MgO) [65], and previously reported values of  $\alpha = 0.77$  and  $\beta = 1.16$  on Cu-wool-like electrodes stabilized by the repetition of the plasma experiments [35]. The changes in the partial pressure dependencies with the catalysts were recognized, but a detailed discussion would require an indepth understanding of the reaction mechanisms. The positive values of the partial pressure of hydrogen on the  $Al_2O_3$  and  $Ni/Al_2O_3$  catalysts are significant for the practical application of the current method because the increase in the hydrogen partial pressure would not result in a decrease in the ammonia formation rate.

The production rate of ammonia was studied as a function of the residence time of the reactant gases. The residence time of the mixture in the reaction port was determined by  $V/F$  (min), where  $V$  is the volume of void space in the reaction port (mL), and  $F$  the total flow rate of the reactants ( $\text{mL min}^{-1}$ ). The results are summarized in Figure 8. The yield of  $NH_3$  increased as the residence time increased, and the rate of  $NH_3$  synthesis became slower for longer times. It should be noted that the degree of decrease of  $NH_3$  synthesis rate on  $Al_2O_3(SC)$  (Figure 8, closed blue) was much higher than that on  $5Ni/Al_2O_3(KC, 773)$  (closed red), although the reason for the difference is not clear yet.



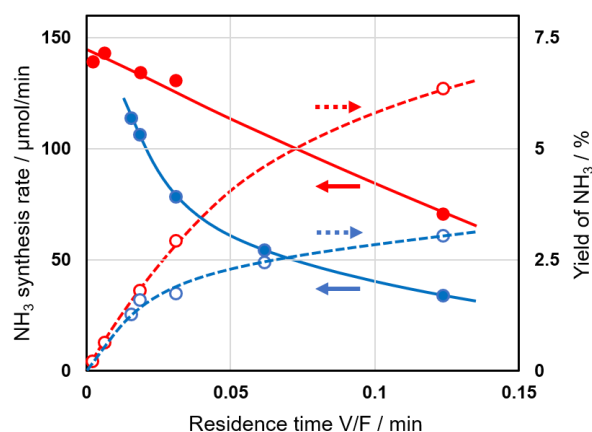


**Figure 8.** Dependence of the synthesis rate (closed) and yield (open) of ammonia on the residence time (V/F) of the reactants gases using  $\text{Al}_2\text{O}_3(\text{SC})$  (blue) and  $5\text{Ni}/\text{Al}_2\text{O}_3(\text{KC}, 773)$  (red) catalysts. Reaction conditions: applied voltage, 6 kV; frequency, 50 kHz; electrode length, 25–150 mm; volume of reaction port (V), 0.515–3.09 mL (the volume was calculated based on the degree of void space (0.52) and the volume of catalyst bed); total flow rate (F), 25–200  $\text{mL min}^{-1}$ ;  $\text{H}_2/\text{N}_2 = 1$ .

The correlation was analyzed using the following equations,

$$\frac{dx}{dt} = r_0 - k_d x \quad (2)$$

$$x = (r_0/k_d)(1 - \exp(-k_d t)) \quad (3)$$

Here, we assumed that the formation rate on the catalyst was constant ( $r_0$  ( $\text{min}^{-1}$ )) because the changes in the partial pressures of  $\text{N}_2$  and  $\text{H}_2$  were small before and after the reaction, and both pressures could be treated as being approximately constant. Additionally, the decomposition rate of ammonia was proportional to the rate constant ( $k_d$  ( $\text{min}^{-1}$ )) and the partial pressure of produced ammonia ( $x$  (-)). Equation (2) was thus formulated and converted to Equation (3) by integration. We applied a least-squares method to determine the parameters of  $\text{Al}_2\text{O}_3(\text{SC})$  and  $5\text{Ni}/\text{Al}_2\text{O}_3(\text{KC}, 773)$ .  $r_0$  and  $k_d$  were 0.73 and 8.4  $\text{min}^{-1}$  for the former and 1.10 and 8.4  $\text{min}^{-1}$  for the latter. We have already reported that the  $r_0$  and  $k_d$  values of the stabilized Cu-wool catalyst were 0.268 and 8.9  $\text{min}^{-1}$ , respectively [38], which showed a significant increase in the  $r_0$  value and a nearly unchanged  $k_d$  value from the values of 0.097 and 8.4  $\text{min}^{-1}$  of the fresh Cu-wool catalyst [39]. The current values determined for  $\text{Al}_2\text{O}_3(\text{SC})$  and  $5\text{Ni}/\text{Al}_2\text{O}_3(\text{KC}, 773)$  indicated further increases in the  $r_0$  values and again unchanged  $k_d$  values. As shown in Figure 8, the maximum ammonia yields were achieved at a residence time of 0.12 min within the current experimental conditions and were 3.0% and 6.3% on  $\text{Al}_2\text{O}_3(\text{SC})$  and  $5\text{Ni}/\text{Al}_2\text{O}_3(\text{KC}, 773)$ .

### 3. Materials and Methods

#### 3.1. Experimental Methods

A copper rod with an 8 mm diameter was employed as the inner electrode in the plasma experiments. The quartz tubular reactor and electrodes are shown in Figure S1 (in Supporting Information). The outer diameter and the thickness of the quartz tube were 12.7 mm and 1.0 mm, respectively. The outer side of the quartz reactor was surrounded by the outer electrode, which consisted of a copper net. The internal electrode was connected to a high-voltage power supply, and the outer electrode acted as a grounded electrode. Oxide catalysts were mounted between the quartz tube and the inner electrode, as shown in Figure S1B. The weight of the catalyst used in the experiment varied depending on the bulk density, and was approximately 2.64–3.85 g. All experiments were performed at atmospheric pressure without heating. A mixture of  $\text{N}_2$  and  $\text{H}_2$  was flowed into the reactor from the top

of the reactor, and the exit gas was delivered to a dilute  $\text{H}_2\text{SO}_4$  aqueous solution to gather the produced ammonia. Typical reaction conditions included an applied voltage of 6 kV and a frequency of 50 kHz for the reaction port (Figures S2 and S3), which was 150 mm in length. A mixture of  $\text{H}_2/\text{N}_2 = 1$  was flowed into the reactor at a flow rate of  $100 \text{ mL min}^{-1}$ , unless otherwise stated. It is important to note that the level of ammonia produced in the current reaction system somewhat varied with the reaction time. The average production rates and yields of ammonia at 60–120 min of reaction time were used to compare the catalytic activity of the respective catalysts. The ammonia yield and the production rate were calculated based on the supplied nitrogen molecules as follows:

$$\text{Yield of ammonia (\%)} = 100 \times \text{conc. of NH}_3 \text{ produced (mol min}^{-1}\text{)} / 2 \times \text{conc. of N}_2 \text{ supplied (mol min}^{-1}\text{)} \quad (4)$$

$$\text{Production rate of ammonia (\mu mol min}^{-1}\text{)} = \text{amount of ammonia produced} \\ \text{in the predetermined time (\mu mol)/sampling interval (min)} \quad (5)$$

### 3.2. Materials

Alumina samples,  $\text{Al}_2\text{O}_3$ , were commercially obtained from Strem Chemicals Inc. (Newburyport, MA., USA) (abbreviated as SC) or Kanto Chemical Co. (Tokyo, Japan) (KC), both of which were of  $\gamma$ -type. The former was in powder form and possessed a BET surface area of  $200.1 \text{ m}^2\text{g}^{-1}$ , and the latter was granular and exhibited  $238.3 \text{ m}^2\text{g}^{-1}$ . Although the surface areas of these substances were slightly different, they were used for the present experiments without distinction (SC and KC are shown in the sample names). Ni-, Fe-, and Ru-supported alumina samples were prepared by a conventional impregnation method using  $\text{Ni}(\text{NO}_3)_2 \cdot 6\text{H}_2\text{O}$ ,  $\text{Fe}_2(\text{NO}_3)_3 \cdot 9\text{H}_2\text{O}$ , and  $\text{Ru}_3(\text{CO})_{12}$ , respectively. The metal loadings were 0.5–20.0 wt% metal. The granular  $\text{Al}_2\text{O}_3$ (KC) was ground into 0.3–0.6 mm particles before loading the active component. The alumina carriers, SC and KC, were dropped into the solutions and the metal species were supported by an impregnation method at 353 K. All catalysts were dried at 393 K overnight and calcined at 773–1073 K for 4 h in air. The calcination temperature is shown in the respective sample names (in Kelvin). After the calcination, the grain sizes of metal/ $\text{Al}_2\text{O}_3$ (SC) were adjusted to 0.3–0.6 mm for use in catalytic runs by compression molding. The compression-molded catalyst was occasionally powdered during the plasma experiment. The pulverization and uneven distribution of the catalyst in the reaction tube made the plasma experiment difficult. To avoid such annoying conditions, most of the experiments in this study were carried out using ground  $\text{Al}_2\text{O}_3$ (KC) as a carrier.

When the sample was filled in a reaction tube, the volume of voids between the catalyst particles was actually measured. The ratio of the void volume to the catalyst bed volume was 0.52, which was used for the calculation of the residence time of reactant gases.

### 3.3. Characterization of Catalysts

The structure of the prepared catalyst was confirmed by X-ray diffraction (XRD) analysis before and after the plasma experiment, in which a Rigaku Ultima IV X-ray diffractometer (Akishima, Tokyo, Japan) with  $\text{Cu K}\alpha$  (40 kV, 40 mA) radiation and a Ni filter was used. X-ray photoelectron spectroscopy (XPS) spectra of nickel were also measured to determine the chemical binding energies and valence states of nickel using a JEOL JPS-9010TR spectrometer (Akishima, Tokyo, Japan) ( $\text{Mg K}\alpha$ ) before and after the plasma experiments. In the latter, the samples were transferred from the reaction port in the plasma reactor to the measurement chamber using a nitrogen box.

## 4. Conclusions

Alumina-supported nickel is a novel and very effective catalyst for ammonia synthesis using nonthermal atmospheric-pressure plasma. The yield of ammonia from  $\text{H}_2$  and  $\text{N}_2$  reached 6.3% without heating, which is the highest among the values examined at ambient temperature. A computational study indicated that the highest barrier for the ammonia decomposition on Ni was the combination

of activated nitrogen atoms to form a dinitrogen molecule [38]. The current reaction is the reverse of the decomposition reaction, and the nitrogen molecule was activated by a plasma system and not by the catalyst surface, which would result in the good activity of Ni/Al<sub>2</sub>O<sub>3</sub>. The reaction mechanism, including the active species in the gas phase and on the surface, should be investigated in the near future. However, the current results pave the way for a new approach to ammonia synthesis that may be significant for future hydrogen applications.

**Supplementary Materials:** The following are available online at <http://www.mdpi.com/2073-4344/10/5/590/s1>, Figure S1: Overall view and sectional view of the reactor, Figure S2: Waveforms of voltage and current, Figure S3: The Lissajous curves of V(t) and I(t) for the plasma reactions, Table S1: detailed data of Figure 1.

**Author Contributions:** Conceptualization, M.I.; reaction on Ni/Al<sub>2</sub>O<sub>3</sub>, M.H., T.S. and K.S.; reaction on metal oxides, R.H.; reaction on Ni/TiO<sub>2</sub>, H.T.; writing—original draft preparation, review and editing, M.I.; supervision, M.M. All authors have read and agreed to the published version of the manuscript.

**Funding:** This work was supported by Grants-in-Aid from the Japan Society for the Promotion of Science (JSPS, METI, 17H03460) and the New Energy and Industrial Technology Development Organization (NEDO, MITI, 17100665-0).

**Conflicts of Interest:** The authors declare no conflicts of interest.

## References

1. Hara, M.; Kitano, M.; Hosono, H. Ru-Loaded C<sub>12</sub>A<sub>7</sub>:e<sup>−</sup> Electride as a Catalyst for Ammonia Synthesis. *ACS Catal.* **2017**, *7*, 2313–2324. [CrossRef]
2. Abe, H.; Niwa, Y.; Kitano, M.; Inoue, Y.; Sasase, M.; Nakao, T.; Tada, T.; Yokoyama, T.; Hara, M.; Hosono, H. Anchoring Bond Between Ru and N Atoms of Ru/Ca<sub>2</sub>NH Catalyst: Crucial for the High Ammonia Synthesis Activity. *J. Phys. Chem. C* **2017**, *121*, 20900–20904. [CrossRef]
3. Kobayashi, V.; Kitano, M.; Kawamura, S.; Yokoyama, T.; Hosono, H. Kinetic evidence: The rate-determining step for ammonia synthesis over electride-supported Ru catalysts is no longer the nitrogen dissociation step. *Catal. Sci. Technol.* **2017**, *7*, 47–50. [CrossRef]
4. Li, J.; Kitano, M.; Ye, T.; Sasase, M.; Yokoyama, T.; Hosono, H. Chlorine-Tolerant Ruthenium Catalyst Derived Using the Unique Anion-Exchange Properties of 12CaO·7Al<sub>2</sub>O<sub>3</sub> for Ammonia Synthesis. *ChemCatChem* **2017**, *9*, 3078–3083. [CrossRef]
5. Kitano, M.; Inoue, Y.; Sasase, M.; Kishida, K.; Kobayashi, Y.; Nishiyama, K.; Tada, T.; Kawamura, S.; Yokoyama, T.; Hara, M.; et al. Self-Organized Ruthenium-Barium Core-Shell Nanoparticles on a Mesoporous Calcium Amide Matrix for Efficient Low-Temperature Ammonia Synthesis. *Angew. Chem. Int. Ed.* **2018**, *57*, 2648–2652. [CrossRef]
6. Ogo, S.; Sekine, Y. Catalytic Reaction Assisted by Plasma or Electric Field. *Chem. Rec.* **2017**, *17*, 726–738. [CrossRef]
7. Murakami, K.; Manabe, R.; Nakatsubo, H.; Yabe, T.; Ogo, S.; Sekine, Y. Elucidation of the role of electric field on low temperature ammonia synthesis using isotopes. *Catal. Today* **2018**, *303*, 271–275. [CrossRef]
8. Manabe, R.; Nakatsubo, H.; Gondo, A.; Murakami, K.; Ogo, S.; Tsuneki, H.; Ikeda, M.; Ishikawa, A.; Nakai, H.; Sekine, Y. Electrocatalytic synthesis of ammonia by surface proton hopping. *Chem. Sci.* **2017**, *8*, 5434–5439. [CrossRef]
9. Ni, J.; Jing, B.; Lin, J.; Lin, B.; Zhao, Z.; Jiang, L. Effect of rare earth on the performance of Ru/MgAl-LDO catalysts for ammonia synthesis. *J. Rare Earths* **2018**, *36*, 135–141. [CrossRef]
10. Ogura, Y.; Sato, K.; Miyahara, S.I.; Kawano, Y.; Toriyama, T.; Yamamoto, T.; Matsumura, S.; Hosokawa, S.; Nagaoka, K. Efficient ammonia synthesis over a Ru/La<sub>0.5</sub>Ce<sub>0.5</sub>O<sub>1.75</sub> catalyst pre-reduced at high temperature. *Chem. Sci.* **2018**, *9*, 2230–2237. [CrossRef]
11. Ma, Z.; Zhao, S.; Xiong, X.; Hu, B.; Song, C. Effect of Graphitic Carbon Nitride on the Electronic and Catalytic Properties of Ru Nanoparticles for Ammonia Synthesis. *Catal. Lett.* **2016**, *146*, 2324–2329. [CrossRef]
12. Yandulov, D.V.; Schrock, R.R. Catalytic reduction of dinitrogen to ammonia at a single molybdenum center. *Science* **2003**, *301*, 76–78. [CrossRef] [PubMed]
13. Shima, T.; Hu, S.; Luo, G.; Kang, X.; Luo, Y.; Hou, Z. Dinitrogen cleavage and hydrogenation by a trinuclear titanium polyhydride complex. *Science* **2013**, *340*, 1549–1552. [CrossRef] [PubMed]

14. Tanabe, Y.; Nishibayashi, Y. Developing more sustainable processes for ammonia synthesis. *Coord. Chem. Rev.* **2013**, *257*, 2551–2564. [\[CrossRef\]](#)
15. Tanaka, H.; Nishibayashi, Y.; Yoshizawa, K. Interplay between Theory and Experiment for Ammonia Synthesis Catalyzed by Transition Metal Complexes. *Acc. Chem. Res.* **2016**, *49*, 987–995. [\[CrossRef\]](#)
16. Kuriyama, S.; Arashiba, K.; Nakajima, K.; Matsuo, Y.; Tanaka, H.; Ishii, K.; Yoshizawa, K.; Nishibayashi, Y. Catalytic transformation of dinitrogen into ammonia and hydrazine by iron-dinitrogen complexes bearing pincer ligand. *Nat. Commun.* **2016**, *7*, 12181. [\[CrossRef\]](#)
17. Amar, I.A.; Lan, R.; Petit, C.T.G.; Tao, S. Solid-state electrochemical synthesis of ammonia: A review. *J. Solid State Electrochem.* **2011**, *15*, 1845–1860. [\[CrossRef\]](#)
18. Giddey, S.; Badwal, S.P.S.; Kulkarni, A. Review of electrochemical ammonia production technologies and materials. *Int. J. Hydrogen Energy* **2013**, *38*, 14576–14594. [\[CrossRef\]](#)
19. Cherkasov, N.; Ibadon, A.O.; Fitzpatrick, P. A review of the existing and alternative methods for greener nitrogen fixation. *Chem. Eng. Process.* **2015**, *90*, 24–33. [\[CrossRef\]](#)
20. Khoenkhon, N.; de Bruin, B.; Reek, J.N.H.; Dzik, W.I. Reactivity of Dinitrogen Bound to Mid- and Late-Transition-Metal Centers. *Eur. J. Inorg. Chem.* **2015**, *2015*, 567–598. [\[CrossRef\]](#)
21. Saadatjou, N.; Jafari, A.; Sahebdehfar, S. Ruthenium Nanocatalysts for Ammonia Synthesis: A Review. *Chem. Eng. Commun.* **2015**, *202*, 420–448. [\[CrossRef\]](#)
22. Klinsrisuk, S.; Irvine, J.T.S. Electrocatalytic ammonia synthesis via a proton conducting oxide cell with BaCe<sub>0.5</sub>Zr<sub>0.3</sub>Y<sub>0.16</sub>Zn<sub>0.04</sub>O<sub>3-δ</sub> electrolyte membrane. *Catal. Today* **2017**, *286*, 41–50. [\[CrossRef\]](#)
23. Kosaka, F.; Noda, N.; Nakamura, T.; Otomo, J. In situ formation of Ru nanoparticles on La<sub>1-x</sub>Sr<sub>x</sub>TiO<sub>3</sub>-based mixed conducting electrodes and their application in electrochemical synthesis of ammonia using a proton-conducting solid electrolyte. *J. Mater. Sci.* **2017**, *52*, 2825–2835. [\[CrossRef\]](#)
24. Bai, M.; Zhang, Z.; Bai, X.; Bai, M.; Ning, W. Plasma synthesis of ammonia with a microgap dielectric barrier discharge at ambient pressure. *IEEE Trans. Plasma Sci.* **2003**, *31*, 1285–1291. [\[CrossRef\]](#)
25. Neyts, E.C. Plasma-Surface Interactions in Plasma Catalysis. *Plasma Chem. Plasma Process.* **2016**, *36*, 185–212. [\[CrossRef\]](#)
26. Neyts, E.C.; Ostrikov, K.; Sunkara, M.K.A. Bogaerts, Plasma Catalysis: Synergistic Effects at the Nanoscale. *Chem. Rev.* **2015**, *115*, 13408–13446. [\[CrossRef\]](#)
27. Whitehead, J.C. Plasma-catalysis: The known knowns, the known unknowns and the unknown unknowns. *J. Phys. D Appl. Phys.* **2016**, *49*, 243001. [\[CrossRef\]](#)
28. Nakajima, J.; Sekiguchi, H. Synthesis of ammonia using microwave discharge at atmospheric pressure. *Thin Solid Films* **2008**, *516*, 4446–4451. [\[CrossRef\]](#)
29. Uyama, H.; Matsumoto, O. Synthesis of ammonia in high-frequency discharges. *Plasma Chem. Plasma Process.* **1989**, *9*, 13–24. [\[CrossRef\]](#)
30. Uyama, H.; Matsumoto, O. Synthesis of ammonia in high-frequency discharges. II. Synthesis of ammonia in a microwave discharge under various conditions. *Plasma Chem. Plasma Process.* **1989**, *9*, 421–432. [\[CrossRef\]](#)
31. Bai, M.; Zhang, Z.; Bai, M.; Bai, X.; Gao, H. Synthesis of ammonia using CH<sub>4</sub>/N<sub>2</sub> plasmas based on micro-gap discharge under environmentally friendly condition. *Plasma Chem. Plasma Process.* **2008**, *28*, 405–414. [\[CrossRef\]](#)
32. Peng, P.; Cheng, Y.; Hatzenbeller, R.; Addy, M.; Zhou, N.; Schiappacasse, C.; Chen, D.; Zhang, Y.; Anderson, E.; Liu, Y.; et al. Ru-based multifunctional mesoporous catalyst for low-pressure and non-thermal plasma synthesis of ammonia. *Int. J. Hydrogen Energy* **2017**, *42*, 19056–19066. [\[CrossRef\]](#)
33. van Helden, J.H.; Wagemans, W.; Yagci, G.; Zijlmans, R.A.B.; Schram, D.C.; Engeln, R.A.H.; Lombardi, G.; Stancu, D.; Ropcke, J. Detailed study of the plasma-activated catalytic generation of ammonia in N<sub>2</sub>-H<sub>2</sub> plasmas. *J. Appl. Phys.* **2007**, *101*, 043305. [\[CrossRef\]](#)
34. Mizushima, T.; Mastumoto, K.; Ohkita, H.; Kakuta, N. Catalytic effects of metal-loaded membrane-like alumina tubes on ammonia synthesis in atmospheric pressure plasma by dielectric barrier discharge. *Plasma Chem. Plasma Process.* **2007**, *27*, 1–11. [\[CrossRef\]](#)
35. Gomez-Ramirez, A.; Cotrino, J.; Lambert, R.M.; Conzalez-Elipe, A.R. Efficient synthesis of ammonia from N<sub>2</sub> and H<sub>2</sub> alone in a ferroelectric packed-bed DBD reactor. *Plasma Sources Sci. Technol.* **2015**, *24*, 06501. [\[CrossRef\]](#)

36. Gomez-Ramirez, A.; Montoro-Damas, A.; Cotrino, J.; Lambert, R.M.; Conzalez-Elipe, A.R. About the enhancement of chemical yield during the atmospheric plasma synthesis of ammonia in a ferroelectric packed bed reactor. *Plasma Process. Polym.* **2017**, *14*, e1600081. [\[CrossRef\]](#)
37. Kim, H.; Teramoto, Y.; Ogata, A.; Takagi, H.; Nanba, T. Plasma Catalysis for Environmental Treatment and Energy Applications. *Plasma Chem Plasma Process* **2016**, *36*, 45–72. [\[CrossRef\]](#)
38. Aihara, K.; Akiyama, M.; Deguchi, T.; Tanaka, M.; Hagiwara, R.; Iwamoto, M. Remarkable catalysis of a wool-like copper electrode for  $\text{NH}_3$  synthesis from  $\text{N}_2$  and  $\text{H}_2$  in non-thermal atmospheric plasma. *Chem. Commun.* **2016**, *52*, 13560–13563. [\[CrossRef\]](#)
39. Iwamoto, M.; Akiyama, M.; Aihara, K.; Deguchi, T. Ammonia Synthesis on Wool-Like Au, Pt, Pd, Ag, or Cu Electrode Catalysts in Nonthermal Atmospheric-Pressure Plasma of  $\text{N}_2$  and  $\text{H}_2$ . *ACS Catal.* **2017**, *7*, 6924–6929. [\[CrossRef\]](#)
40. Muroyama, H.; Saburi, C.; Matsui, T.; Eguchi, K. Ammonia decomposition over  $\text{Ni/La}_2\text{O}_3$  catalyst for on-site generation of hydrogen. *Appl. Catal. A Gen.* **2012**, *443–444*, 119–124. [\[CrossRef\]](#)
41. Duan, X.; Qian, G.; Liu, Y.; Ji, J.; Zhou, X.; Chen, D.; Yuan, W. Structure sensitivity of ammonia decomposition over Ni catalysts: A computational and experimental study. *Fuel Process. Technol.* **2013**, *108*, 112–117. [\[CrossRef\]](#)
42. Sato, K.; Abe, N.; Kawagoe, T.; Miyahara, S.; Honda, K.; Nagaoka, K. Supported Ni catalysts prepared from hydrotalcite-like compounds for the production of hydrogen by ammonia decomposition. *Int. J. Hydrogen Energy* **2017**, *42*, 6610–6617. [\[CrossRef\]](#)
43. Polanski, J.; Bartzak1, P.; Ambrozkiwicz1, W.; Sitko1, R.; Siudyga, T.; Mianowski, A.; Szade, J.; Balin, K.; Leltko, J. Ni-Supported Pd Nanoparticles with Ca Promoter: A New Catalyst for Low-Temperature Ammonia Cracking. *PLoS ONE* **2015**. [\[CrossRef\]](#) [\[PubMed\]](#)
44. Li, L.; Chen, F.; Shao, J.; Dai, Y.; Ding, J.; Tang, Z. Attapulgite clay supported Ni nanoparticles encapsulated by porous silica: Thermally stable catalysts for ammonia decomposition to  $\text{CO}_x$  free hydrogen. *Int. J. Hydrogen Energy* **2016**, *41*, 21157–21165. [\[CrossRef\]](#)
45. Atsumi, R.; Noda, R.; Takagi, H.; Vecchione, L.; Carlo, A.D.; Del Prete, Z.; Kuramoto, K. Effects of Steam on  $\text{Ni/Al}_2\text{O}_3$  Catalysts for Ammonia Decomposition. *Ind. Eng. Chem. Res.* **2014**, *53*, 17849–17853. [\[CrossRef\]](#)
46. Zheng, W.; Zhang, J.; Ge, Q.; Xu, H.; Li, W. Effects of  $\text{CeO}_2$  addition on  $\text{Ni/Al}_2\text{O}_3$  catalysts for the reaction of ammonia decomposition to hydrogen. *Appl. Catal. B Environ.* **2008**, *80*, 98–105. [\[CrossRef\]](#)
47. Hargreaves, J.S.J.; Mckay, D. A comparison of the reactivity of lattice nitrogen in  $\text{Co}_3\text{Mo}_3\text{N}$  and  $\text{Ni}_2\text{Mo}_3\text{N}$  catalysts. *J. Mol. Catal. A Chem.* **2009**, *305*, 125–129. [\[CrossRef\]](#)
48. Taylor, D.W.; Smith, P.J.; Dowdenc, D.A.; Kemball, C.; Whan, D.A. Ammonia synthesis and related reactions over iron-cobalt and iron-nickel alloy catalysts. Part I. Catalysts reduced at 853 K. *Appl. Catal.* **1982**, *3*, 161–176. [\[CrossRef\]](#)
49. Jacobsen, C.J.H. Novel class of ammonia synthesis catalysts. *Chem. Commun.* **2000**, 1057–1058. [\[CrossRef\]](#)
50. Abghoui, Y.; Skulason, E. Computational Predictions of Catalytic Activity of Zincblende (110) Surfaces of Metal Nitrides for Electrochemical Ammonia Synthesis. *J. Phys. Chem. C* **2017**, *121*, 6141–6151. [\[CrossRef\]](#)
51. Ouyang, B.; Zhang, Y.; Zhang, Z.; Fan, H.J.; Rawat, R.S. Nitrogen-Plasma-Activated Hierarchical Nickel Nitride Nanocorals for Energy Applications. *Small* **2017**, *13*, 1604265. [\[CrossRef\]](#) [\[PubMed\]](#)
52. Spreafico, C.; Karim, W.; Ekinci, Y.; van Bokhoven, J.A.; VandeVondele, J. Hydrogen Adsorption on Nanosized Platinum and Dynamics of Spillover onto Alumina and Titania. *J. Phys. Chem. C* **2017**, *121*, 17862–17872. [\[CrossRef\]](#)
53. Karim, W.; Spreafico, C.; Kleibert, A.; Gobrecht, J.; VandeVondele, J.; Ekinci, Y.; van Bokhoven, J.A. Catalyst support effects on hydrogen spillover. *Nature* **2017**, *541*, 69–74. [\[CrossRef\]](#) [\[PubMed\]](#)
54. Li, G.; Hu, L.; Hill, J.M. Comparison of reducibility and stability of alumina-supported Ni catalysts prepared by impregnation and co-precipitation. *Appl. Catal. A Gen.* **2006**, *301*, 16–24. [\[CrossRef\]](#)
55. Akande, A.J.; Idem, R.O.; Dalai, A.K. Synthesis, characterization and performance evaluation of  $\text{Ni/Al}_2\text{O}_3$  catalysts for reforming of crude ethanol for hydrogen production. *Appl. Catal. A Gen.* **2005**, *287*, 159–175. [\[CrossRef\]](#)
56. Ragupathi, C.; Bijaya, J.J.; Surendhar, P.; Kennedy, L.J. Comparative investigation of nickel aluminate ( $\text{NiAl}_2\text{O}_4$ ) nano and microstructures for the structural, optical and catalytic properties. *Polyhedron* **2014**, *72*, 1–7. [\[CrossRef\]](#)

57. El-Shobaky, G.A.; Al-Noaimi, A.N.; Saber, T.M.H. Structure and catalytic activity of nickel oxide/alumina (NiO/Al<sub>2</sub>O<sub>3</sub>) prepared by impregnation or coprecipitation. *Bull. Soc. Chim. France* **1987**, 930–934, CODEN BSCFAS.
58. Jeevanandam, P.; Koltypin, Y.; Gedanken, A. Preparation of nanosized nickel aluminate spinel by a sonochemical method. *Mater. Sci. Eng. B* **2002**, 90, 125–132. [[CrossRef](#)]
59. Zhang, Q.; Wu, T.; Zhang, P.; Qi, R.; Huang, R.; Song, X.; Gao, L. Facile synthesis of hollow hierarchical Ni/γ-Al<sub>2</sub>O<sub>3</sub> nanocomposites for methane dry reforming catalysis. *RSC Adv.* **2014**, 4, 51184–51193. [[CrossRef](#)]
60. Inoue, H.; Hatanaka, N.; Kidena, K.; Murata, S.; Nomura, M. Reforming of Methane with Carbon Dioxide over Nickel-loaded Zeolite Catalysts. *J. Jpn. Petroleum Inst.* **2002**, 45, 314–320. [[CrossRef](#)]
61. Xiang, L.; Gong, Y.L.; Li, J.C.; Wang, Z.W. Influence of hydrothermal modification on the properties of Ni/Al<sub>2</sub>O<sub>3</sub> catalyst. *Appl. Surf. Sci.* **2004**, 239, 94–100. [[CrossRef](#)]
62. Al-Ubaid, A.; Wolf, E.E. Steam reforming of methane on reduced non-stoichiometric nickel aluminate catalysts. *Appl. Catal.* **1988**, 40, 73–85. [[CrossRef](#)]
63. Salagre, P.; Fierro, J.L.G.; Medina, F.; Sueiras, J.E. Characterization of nickel species on several γ-alumina supported nickel samples. *J. Mol. Catal. A Chem.* **1996**, 106, 125–134. [[CrossRef](#)]
64. Zhang, L.; Shu, X.; Zhang, L. Influence of Ni Loading on Catalytic Activity of NiO/γ-Al<sub>2</sub>O<sub>3</sub> for Hydrogenation of Coal Pyrolysis. *Asian J. Chem.* **2013**, 25, 5071–5075. [[CrossRef](#)]
65. Hagen, S.; Barfod, R.; Fehrmann, R.; Jacobsen, C.J.H.; Teunis-sen, H.T.; Chorkendorff, I. Ammonia synthesis with barium-promoted iron–cobalt alloys supported on carbon. *J. Catal.* **2003**, 214, 327–335. [[CrossRef](#)]



© 2020 by the authors. Licensee MDPI, Basel, Switzerland. This article is an open access article distributed under the terms and conditions of the Creative Commons Attribution (CC BY) license (<http://creativecommons.org/licenses/by/4.0/>).